Uncertainty Analysis of a Multiprobe Antenna Measurement System for Full Vehicle Testing

F. Saccardi *AMTA Fellow*, A. Giacomini, *Senior AMTA*, Jaydeep Singh, L. Foged, *AMTA Fellow*
Microwave Vision Italy SRL,
Via dei Castelli Romani 59, 00071, Pomezia, Italy
francesco.saccardi@mvg-world.com

T. Blin, N. Gross
MVG Industries, 13 rue du Zéphyr
Villejust, France
thierry.blin@mvg-world.com

Arthur Romeijer,
Pulsaart by AGC
Rue Louis Blériot 12 , 6041 Gosselies, Belgium
Arthur.Romeijer@agc.com

Abstract— In this paper, we present an overview and comparison of various experimental techniques to identify the room scattering contribution to the overall measurement uncertainty in spherical near-field systems. Our primary objective is to determine the upper bound of the uncertainty due to room scattering in the automotive multi-probe system at the Pulsaart by AGC facility. This facility is designed for comprehensive vehicle testing across a broad frequency range from 64 MHz to 6 GHz. At the lower end of this frequency range, room scattering significantly impacts the overall antenna measurement uncertainty budget, making it crucial to quantify the upper bounds of this error.

The considered experimental techniques to determine the room scattering contributions include measuring the same Antenna Under Test (AUT) at multiple translated positions within the chamber, employing advanced post-processing techniques to eliminate room scattering and identify its effects, and combining both approaches. This activity aims to define the room scattering contribution, particularly at lower frequencies, to the range's overall antenna measurement uncertainty budget.

I. Introduction

Recent developments in vehicular communication technologies demand radiated testing considering the entire vehicle, which typically hosts numerous integrated antennas. In response, automotive antenna measurement systems with high accuracy and rapid measurement speeds have become indispensable [1]-[2].

Spherical Near Field (SNF) testing techniques are the preferred method for automotive applications because they can precisely measure antennas of varying directivities and because of their low spatial footprint [3]-[4]. However, as SNF technology requires a full sampling, the primary limitation of these systems is the corresponding testing time required to meet sampling demands. Multi-Probe Array (MPA) systems address this challenge effectively by capturing multiple sampling points in the same scan position, thereby reducing measurement times, typically by factors of 5 to 10, depending on the frequency band [1]-[2].

One such system is the spherical automotive MPA system installed at the Pulsaart by AGC facility [5]. It is designed for comprehensive vehicle testing across 64 MHz to 6 GHz frequencies. The system features a hemispherical, 12-meter-diameter arch within a compact anechoic chamber, shielded and optimized with an absorber layout for the relevant frequency ranges.

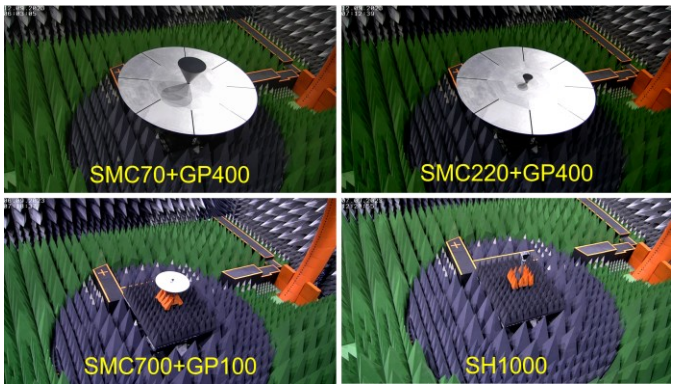

Figure 1. Photos of four (out of seven) antennas measured in the MPA range at Pulsaart by AGC.

This paper presents novel findings from an extensive measurement campaign conducted to refine the uncertainty budget of the system. The campaign mainly focused on the error term associated with the residual reflectivity of the measurement environment, a significant contributor to the overall measurement uncertainty, especially at lower frequencies (e.g., VHF/UHF), where the relative size of anechoic chambers and absorbing materials typically falls short to the wavelength [6]-[7]. As shown in Figure 1. the campaign includes measurements

of several reference antennas across different frequencies and positions to accurately assess the interaction with the measurement environment.

The paper provides preliminary findings from the extensive processing of two dual-ridge horns measured in different positions within the measurement system in the 400MHz to 6GHz frequency range. The different antenna positions are used to estimate the reflectivity uncertainty term. For the first time, three different reflectivity evaluation approaches will be compared.

Standard methods for evaluating the chamber reflectivity for direct FF methods are based on measuring the reflection level of the chamber wall surfaces into the target area or Quiet Zone (QZ) relative to the on-axis direct incident field. These methods are often called the free-space voltage standing wave ratio (VSWR) test [8]. While offering a good measure of the reflections into the measurement area of NF systems, it does not quantify the (positive) effect of the modal expansion-based Near Field to Far Field (NF/FF) transformation [3]-[4] and does not allow an evaluation of the dependency on the Antenna/Device Under Test (AUT/DUT) [3]. Different antenna types will illuminate the chamber differently; thus, the measurement uncertainty due to chamber reflections will differ for different types of antennas. The proposed evaluation directly considers that effect based on comparing and analyzing the antenna patterns obtained from the measurement at different positions including the transformation process.

II. Description of the MPA System

Pulsaart's MPA system is designed to meet the strict requirements of the automotive industry. Its seven-meter diameter turntable can accommodate large vehicles weighing up to three tons. The system includes a lifting column that allows the vehicles to be centred in the coordinate system, helping to reduce the sampling size. The arch, capable of scanning elevations from 0° (i.e. the zenith) to 110° (i.e. 20° below the horizon), allows the capture of antenna radiation patterns below the horizon, which is vital for C-V2X antennas due to their specific operational requirements.

The anechoic chamber is equipped with pyramidal absorbing material of different sizes, including 48 and 60 inches, allowing accurate measurement down to 64MHz. The 6m radius MPA is divided into two semiarches: one with 22 dual-pol probes (5° spacing) for measurements in the 64-400MHz band and one with 111 dual-pol probes (1° spacing) for measurements in the 0.4-6GHz range. The ground floor of the system (also covered by absorbers) is 2.5m below the arch center, and it hosts a turntable used to perform the full 360° azimuth scanning. The so-called orthomodal calibration [3] is periodically performed to equalize the probes' on-axis amplitude and phase response and compensate for their on-axis cx-polarization. Gain calibration is achieved using two types of reference antennas: monocones and dual-ridged horns. These reference antennas are crucial for extracting the absolute realized gain of the AUT (i.e. gain/efficiency substitution technique, [3], [8], [9]). Using a reference antenna with a radiation pattern closely matching the AUT one is good practice to achieve accurate measurements [1]. Monocones are particularly well-suited for automotive applications due to their comparable radiation characteristics.

Such a facility provides rapid antenna measurement capabilities for the automotive sector and industries such as space technology, drone technology, and telecommunications. The possibility of efficiently conducting realized gain radiation pattern measurements is crucial for performance validation and prototyping. These measurements can yield additional figures of merit, such as efficiency, directivity, and polarization, providing comprehensive insights into antenna performance.

III. Measurement Uncertainty Evaluation

Pulsaart MPA is certified ISO17025:2017 for gain measurements across a frequency range from 64 MHz to 6 GHz. The ongoing efforts aim to expand this certification to other figures of merit (pattern, efficiency, polarization, directivity) and refine the current uncertainty budget to ensure the highest standards of accuracy and reliability [10]-[11].

The main objective of this investigation is to refine the reflectivity uncertainty term of the MPA system. For this purpose, several antennas have been selected and measured in different positions within the range. The chosen antennas are monocones mounted on circular ground planes and dual-ridge horns, as shown in Figure 1.

The almost omnidirectional radiation patterns of monocones antennas (i.e. the SMC family from MVG, [12]) provide a significant illumination of the measurement range. Hence, they represent a worst-case scenario. Five different monocone antennas have been considered to cover the system's full frequency range, from 64MHz to 6GHz.

On the other hand, the considered horn antennas (i.e. the SH400 and SH1000 from MVG, [13]) have been selected to assess the effect of the chamber reflectivity in case of higher directive AUT/DUT (approximately 8dBi to 15dBi). The analysis with the horns has been conducted in the 400-6000MHz frequency range. In this paper we focus on the analysis of such horn antennas which peak directivity over frequency is depicted in Figure 2.

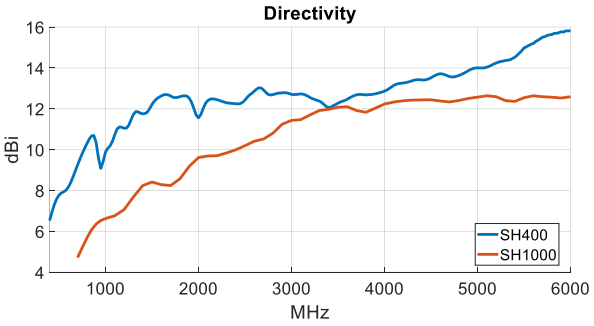

Figure 2. Nominal peak directivity over frequency of the SH400 and SH1000 considered in this investigation.

As mentioned above, all the considered antennas have been measured in different positions within the range to change their interaction with the anechoic chamber. In fact, changing the antenna position generates different scattered/interfering

signals, allowing the assessment of the residual chamber reflectivity by mean of pattern comparison and analysis.

The Equivalent Noise Level (ENL), as defined in equation (1), is a widely accepted metric used to compare two radiation patterns, and quantify their correlation. In this equation, $E_i(\theta, \varphi)$ and $E_j(\theta, \varphi)$ are two radiation patterns to be compared, and RMS is the operator evaluating the Root Mean Square. Due to the hemispherical nature of this MPA, the ENL is always evaluated only up to $\theta = 90°$ in this study.

$$ENL_{ij} = 20\log_{10}\left(RMS\left|\frac{E_i(\theta, \varphi) - E_j(\theta, \varphi)}{E_i(\theta, \varphi)_{MAX}}\right|\right) \quad (1)$$

From the ENL, the corresponding perturbation (ε) at a specific Antenna Pattern Level (APL) can be eveluated with equation (2).

$$\varepsilon = 20log_{10}\left(1 + \frac{10^{ENL_{ij}/20}}{10^{APL/20}}\right) \quad (2)$$

It should be noted that when the same antenna is measured in different positions inside the range, other error terms are also changed besides the measurement errors due to reflections. The main ones are the effect of the probe pattern [14] and the truncation of the scanning area [15]. The complete isolation of the reflectivity term is usually not possible. However, different statistical methods can be applied in order to estimate such an error term.

A. Methods to Extract the Reflectivity Level

Let us assume that the measurement uncertainty deriving from the measurement of the same antenna in different positions (u_{tot}) is given by the Root Square Summation (RSS) of the three uncertainty terms reported in (3)

$$u_{tot} = \sqrt{u_{Probe}^2 + u_{Truncation}^2 + u_{Reflection}^2} \quad (3)$$

With u_{probe} being the uncertainty due to the effect of the probe pattern, $u_{Truncation}$ the one due to the truncation of the spherical scanning area, and $u_{Reflection}$ the one due to the chamber reflectivity.

1) Method #1

The first method relies on applying spatial/modal filtering [16],[17] on the measured pattern to suppress the effect of the reflections as much as possible. MvEcho by MVG [18] is an example of an echo suppression software tool based on spherical wave modal filtering considering the minimum sphere of the antenna. The effectiveness of MvEcho has been demonstrated in several scenarios, especially in the case of the relatively electrically small offset antennas [16]-[19].

In this study, Method#1 is applied in the following way: u_{tot} is first obtained from the computation of the ENL among each pair of measured patterns, without applying MvEcho. The RMS combination of the different ENL is used to provide a global indicator of the correlation among the patterns measured with the different antenna offset (i.e. global ENL defined in equation (4)).

$$ENL_{global} = 20\log_{10}\left(\sqrt{\frac{\sum_{ij} 10^{ENL_{ij}/10}}{N}}\right) \quad (4)$$

The global ENL is then computed considering the radiation patterns processed with MvEcho. Assuming they are not anymore affected by reflections, such a global ENL will account only for the probe pattern and truncation effects ($u_{tot,filtered} = \sqrt{u_{Probe}^2 + u_{Truncation}^2}$). The reflectivity term can hence be estimated by equation (5).

$$u_{Reflection} = \sqrt{u_{tot}^2 - u_{tot,filtered}^2} \quad (5)$$

The limitation of such an approach is mainly due to a possible lack of complete echo suppression during the application of MvEcho (e.g. reflected signals inside the antenna minimum sphere). Although not considered in this work, other reflection suppression techniques, like time gating, can be considered in order to further improve this approach.

2) Method #2

Similar to Method#1, the second method is again based on applying MvEcho to each measured pattern to suppress the effect of the reflected signals as much as possible. In this case, the ENL is computed by considering the spatial/modal filtered pattern and the unfiltered pattern in equation (1). In this way, the ENL provides a direct indication of the chamber reflectivity because the other error terms are common to both patterns considered in the formula. Such an approach has already been used in another analysis [19]. In this investigation, an ENL trace is obtained for each individual offset measurement and then the global ENL is computed again using (4).

3) Method #3

The third method to extract the effect of the chamber reflectivity relies on estimating the uncertainty terms associated with the probe pattern and the truncation of the scanning area using measurement emulations. Once these terms are computed, (5) is inverted by means of $u_{Reflection}$. Like Method #1, u_{tot} is obtained from the global ENL of the different patterns without any filtering applied. In this study, the estimation of $u_{Probe}^2 + u_{Truncation}^2$ is performed using the well-known SWE-based transmission formula [20], which efficiently emulates SNF measurements including the probe effect and the wanted truncation area. Of course, this approach requires the knowledge of the probe pattern with sufficient accuracy.

IV. SH400 Analysis

The first considered antenna for this analysis is the MVG SH400 dual-ridge horn working the 400 – 6000MHz wide frequency range. Table I. reports the considered antenna positions with respect to the origin of the coordinate system (i.e. the center of the arch) with the associated frequency band and angular sampling. Photos of two out of the five antenna positions within the range are shown on the left side of Figure 3.

Figure 4. shows examples of gain radiation patterns at 400, 2000 and 4000MHz of the SH400 measured at different positions with (right) and without (left) MvEcho applied. The ripples in the un-filtered data are basically due to the chamber reflectivity and are significantly suppressed when MvEcho is applied. The differences on the main beam among the different antenna positions observable at 4000MHz after the application of the MvEcho are due to the probe pattern effect, which deviates from an ideal dipole-like pattern at such frequency, and its effect becomes noticeable, especially with the lateral placement of the antenna [14].

TABLE I. SH400 MEASUREMENT CONFIGURATIONS

(X, Y, Z)	Frequency	Δθ	Δφ
(0, 0, 0)m	400 – 6000MHz	1.0°	2.5°
(0, 0, +1.2)m	400 – 5600MHz	1.0°	1.0°
(0, 0, +2.0)m	400 – 3600MHz	1.0°	1.0°
(+1.5, 0, 0)m	400 – 4000MHz	1.0°	1.0°
(+1.2, 0, 0)m	4000 – 6000MHz	1.0°	1.0°

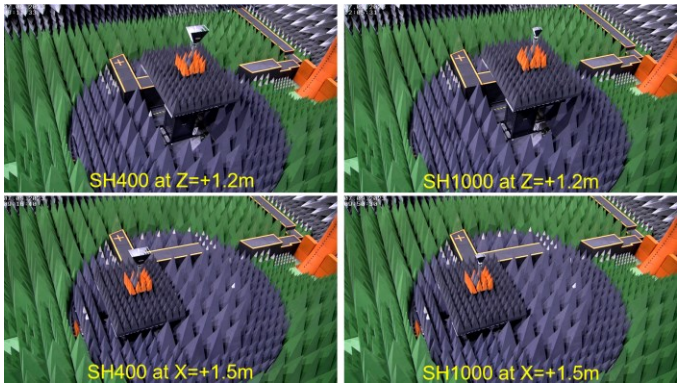

Figure 3. Photos of two (out of five) positions of the SH400 (left) and SH1000 (right) inside the MPA range.

The global ENL with and without MvEcho applied to the measured radiation patterns are reported in Figure 5. As expected, the correlation among the different offset measurements is improved when MvEcho is applied (green trace, lower ENL) because the reflections are significantly suppressed. The increase of the global ENL beyond 2GHz is also expected due to the tapering effect of the measurement probes. According to Method#1 previously described, the reflectivity uncertainty term can be extracted from the delta between the two global ENL (see equation (5)). The extrapolated reflectivity, in terms of the equivalent error signal in four sub-bands, obtained with Method#1 is reported in the second column of Table II.

Figure 6. reports the ENL computed considering in equation (1) the radiation patterns with and without MvEcho applied. The different traces are associated with the measurements of the SH400 performed in different positions. Such information is used to derive the reflectivity uncertainty with Method#2, as described above. The estimated reflectivity levels with Method#2 are reported in the third column of Table II.

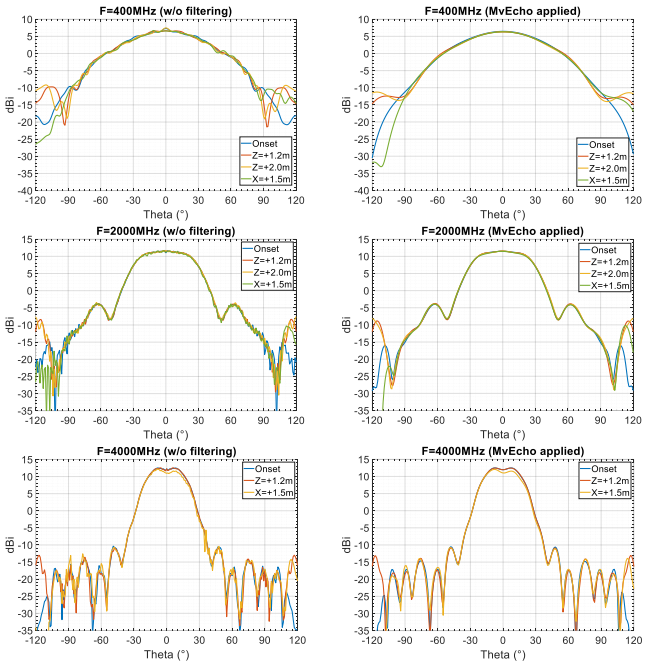

Figure 4. Measured gain radiation patterns of the SH400 with (right) and without (left) MvEcho applied.

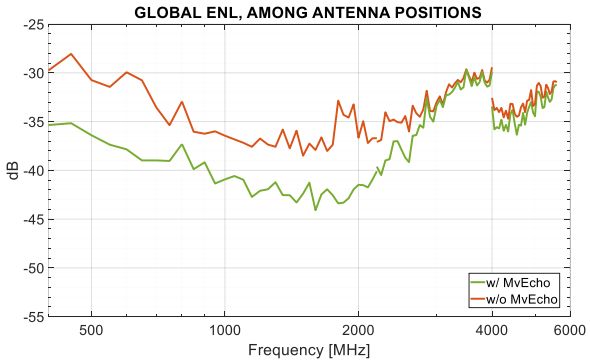

Figure 5. SH400 measurements: Global ENL with and without MvEcho.

Finally, the reflectivity levels obtained with Method #3 are reported in the fourth column of Table II. As previously explained, such a method requires emulating the probe and truncation uncertainty terms ($u^2_{Probe} + u^2_{Truncation}$). For this purpose, measurement emulations of the SH400 in the same positions as the actual measurements have been performed with the SWE-based transmission formula. The considered dual-

polarized probe model is obtained from a separate measurement of a representative mock-up of the MPA [21]. The same truncation of the scanning area of the actual MPA has also been considered ($\theta_{max} = 110°$).

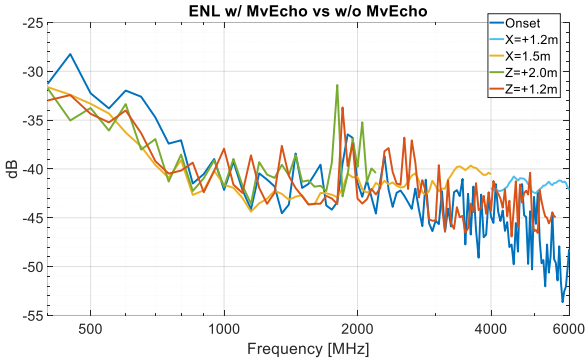

Figure 6. SH400 measurements: ENL obtained from the patterns with and without MvEcho.

TABLE II. ESTIMATED REFLECTIVITY FROM THE SH400 MEASUREMENTS WITH THE DIFFERENT PROPOSED METHODS

Band [MHz]	Method #1	Method #2	Method#3
400-800	-32.1	-34.3	-33.04
800-2200	-37.6	-40.5	-41.62
2200-4000	-39.8	-41.9	-34.86
4000-6000	-39.6	-43.4	-39.41

V. SH1000 ANALYSIS

Similar measurements performed with the SH400 have also been conducted with the SH1000, as depicted in Table III. and on the right side of Figure 3. The SH1000 is an approximately 2.5-time scaled version of the SH400, nominally working in the 1-18GHz frequency band. Being smaller than the SH400, the SH1000 provides more illumination of the measurement environment (see directivity comparison in Figure 2.). Hence, higher reflectivity estimations are expected when compared to the SH400 at the same frequencies.

TABLE III. SH1000 MEASUREMENT CONFIGURATIONS

(X, Y, Z)	Frequency	Δθ	Δφ
(0, 0, 0)m	1000 – 6000MHz	1.0°	2.5°
(0, 0, +2.0)m	1000 – 3800MHz	1.0°	1.0°
(0, 0, +1.2)m	4000 – 6000MHz	1.0°	1.0°
(+1.5, 0, 0)m	1000 – 4000MHz	1.0°	1.0°
(+1.2, 0, 0)m	4000 – 6000MHz	1.0°	1.0°

The global ENL obtained from the radiation patterns of the SH1000 with and without MvEcho applied are shown in Figure 7. Similar to the previous analysis with the SH400, the two global ENLs significantly differ at lower frequencies, where the reflectivity is expected to be more significant. Moreover, the increase of the global ENL beyond 2GHz is again due to the probe effect, which pattern becomes more directive, increasing its tapering effect on the measured antenna pattern. Such global ENL has been used to derive the reflectivity level with Method#1.

The ENL obtained for each measurement of the SH1000 comparing the patterns with and without the modal filtering (MvEcho) are reported in Figure 8. Such ENL has been used to derive the reflectivity level with Method#2.

Table IV. summarizes the reflectivity levels obtained from the offset measurements of the SH1000 with the different reflectivity evaluation methods.

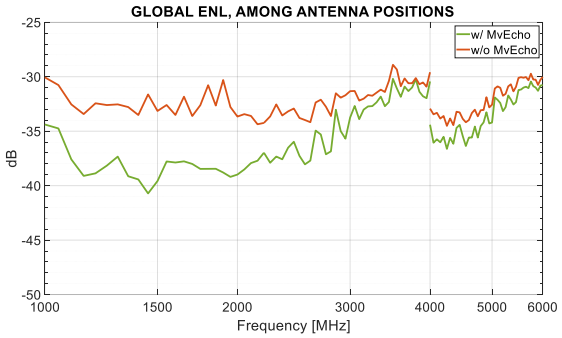

Figure 7. SH1000 measurements: Global ENL with and without MvEcho (Method #1).

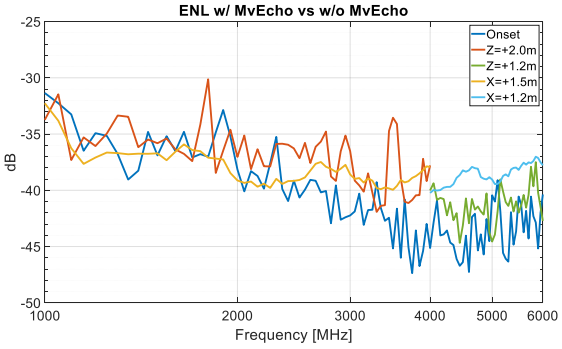

Figure 8. SH1000 measurements: ENL obtained from the patterns with and without MvEcho (Method #2).

TABLE IV. ESTIMATED REFLECTIVITY FROM THE SH1000 MEASUREMENTS WITH THE DIFFERENT PROPOSED METHODS

Band [MHz]	Method #1	Method #2	Method#3
1000-2200	-33.9	-35.7	-36.95
2200-4000	-36.6	-38.8	-34.16
4000-6000	-38.0	-40.5	-38.73

VI. DISCUSSION OF THE RESULTS

As expected, the reflectivity levels obtained with the SH1000 arehigher than those obtained with the SH400. That is due to the broader radiation pattern of the SH1000, which illuminates the measurement environment more. The importance of evaluating such an uncertainty term using different antenna types is

highlighted. How the chamber reflections influence the final measurement of the AUT/DUT, depends on the AUT/DUT itself. Hence, the availability of different uncertainties obtained considering different "typical" antennas allows us to choose the one that most fits the AUT/DUT.

The reflectivity levels obtained with the different methods are pretty in line with each other. However, in some cases, some differences can be observed. Although the authors are currently in the process of better understanding such differences, some preliminary considerations can be made.

It can be observed that Method#1 is more conservative than Method#2. This is likely due to the ENL metric of Method#1 comparing different measurement positions of the same antenna, where pattern differences are maximized. In contrast, Method#2 applies the ENL metrics on two patterns deriving from the same measurement but processed differently (i.e., with and without modal filtering). This likely does not capture the full effect of reflections. The almost constant deviation of approximately 2-3 dB between Method#1 and Method#2 suggests that both are valid methodologies in chamber reflection evaluation but with different confidence levels. Differences still need to be examined further. That is important to quantify as Method#1 may not be feasible in all cases, and Method#2 may be the only solution for a given scenario.

The reflectivity levels obtained with Method#3 agree very well with those obtained with Method#1 in the 400-800 MHz and 4-6 GHz sub-bands, indicating that the emulation of the other uncertainty contributions, such as probe pattern and truncation effects, aligns with the actual ones. However, non-explained deviations are observed in other sub-bands. Further investigations are needed to understand the root cause of these differences, and a refinement of the performed measurement emulations may be necessary.

VII. Conclusions

According to the IEEE standards [3] and [8], simultaneous translation of both the AUT and the probe to the chamber is recommended to determine the room scattering effect. This is in most cases not a feasible approach due to the physical constraints of many systems, particularly in the Pulsaart facility. In this paper, we have examined the chamber scattering by translating the movement of the AUT and post-processing. The various experimental investigations of this error are in good agreement with each other and form a solid basis for estimating an upper error bound for this facility's overall antenna measurement uncertainty budget.

Based on the findings from this experimental activity, the overall uncertainty budget of the facility will be refined by isolating and quantifying the room scattering component. This paper presents preliminary results from measurements of two horn antennas positioned at different locations within the 400 MHz to 6 GHz frequency range. The investigation will be extended to include similar measurements of monocone antennas, covering the full frequency range of the facility (64 MHz to 6 GHz).

References

[1] Foged, L.J and M. Sierra-Castaner, Modern Automotive Antenna Measurements, Artech House, Boston, Massachusetts, 2022.

[2] P. Noren, Ph. Garreau, L. J. Foged, "State of the art spherical near-field antenna test systems for full vehicle testing", 6th European Conference on Antennas and Propagation, EuCAP 2012, March 2012, Prague, Czech Republic;

[3] IEEE Std 1720-2012 "Recommended Practice for Near-Field Antenna Measurements"

[4] J. E. Hansen (ed.), Spherical Near-Field Antenna Measurements, Peter Peregrinus Ltd., on behalf of IEE, London, United Kingdom, 1988

[5] https://www.pulsaart.com/

[6] F. Saccardi, A. Giacomini, N. Gross, T. Blin, P.O. Iversen, L. J. Foged, "VHF/UHF Antenna Measurements Based on Multi Probe Array Technology" EuCAP 2024, Glasgow, Scotland.

[7] A. Giacomini, V. Schirosi, F. Saccardi, F. Rossi, N. J. G. Fonseca, P. de Maagt, L. J. Foged "Measurements of Low Gain Antennas at VHF Frequencies for Space-Based AIS Applications" EuCAP 2017, 19-24 March, Paris, France

[8] IEEE Std 149-2021 "IEEE Standard Test Procedures for Antennas"

[9] F. Saccardi, F. Mioc, A. Giacomini, A. Scannavini, L. J. Foged, J. Estrada, P. O. Iversen, M. Edgerton, J. A. Graham, "Accurate Calibration of Truncated Spherical Near Field Systems with Different Ground Floors using the Substitution Technique" AMTA 2019, October 6-11, San Diego, USA

[10] A. C. Newell, "Error analysis techniques for planar near-field measurements," in IEEE Transactions on Antennas and Propagation, vol. 36, no. 6, pp. 754-768, June 1988, doi: 10.1109/8.1177.

[11] ISO/IEC Guide 98-3:2008(E), Uncertainty of Measurement—Part 3: Guide to the Expression of Uncertainty in Measurement (GUM: 1995), 2008.

[12] https://www.mvg-world.com/en/products/antennas/reference-antennas/monocones

[13] https://www.mvg-world.com/en/products/antennas/reference-antennas/dual-ridge-horns

[14] F. Saccardi, A. Giacomini, L. J. Foged, T. Blin "Experimental Validation of Full Probe Correction Technique using Wideband and Dual-Polarized Probes in Spherical NF Antenna Measurements" AMTA 2021, October 24-29, Daytona Beach, FL, USA

[15] F. Saccardi, F. Rossi, L. Scialacqua, L. J. Foged, "Truncation Error Mitigation in Free-Space Automotive Partial Spherical Near Field Measurements", AMTA 2017, 15-20 October, Atlanta, GA, USA

[16] L. J. Foged, L. Scialacqua, F. Mioc, F. Saccardi, P. O. Iversen, L. Shmidov, R. Braun, J. L. Araque Quijano, G. Vecchi " Echo Suppresion by Spatial Filtering Techniques in Advanced Planar and Spherical NF Antenna Measurements ", AMTA Symposium, October 2012, Seattle, Washington, USA

[17] "Post-processing Techniques in Antenna Measurement", edited by M. Sierra Castañer and Lars. J. Foged, SciTech Publishing, The Institution of Engineering and Technology, London, UK ISBN 978-1-78561-537-5.

[18] https://www.mvg-world.com/en/products/antenna-measurement/software/mv-echo

[19] F. D'Agostino, F. Ferrara, C. Gennarelli, R. Guerriero, M.A. Saporetti, F.Saccardi, L.J. Foged, D. Trenta "Echo Reduction Properties of Fast Non-Redundant Planar NF Sampling Methodologies" EuCAP 2020, 15 - 20 March, Copenhagen, Denmark

[20] F. Saccardi, A. Giacomini, L. J. Foged "Accurate Evaluation of Antenna Measurement Range Performance with the SWE Transmission Formula" AMTA 2023, October 8-13, Seattle, WA, USA

[21] F. Saccardi, A. L. J. Foged, Gross, T. Blin, P.O. Iversen, R. Braun, L. Shmidov, M. He, C. Chen, X. Bland "Experimental Validation of Linear Multiprobe Arrays for Fast and Accurate PNF Antenna Characterizations" AMTA 23, 7-13 October, Seattle, WA, USA